

## Ultra-high strain in epitaxial silicon carbide nanostructures utilizing residual stress amplification

Hoang-Phuong Phan, Tuan-Khoa Nguyen, Toan Dinh, Ginnosuke Ina, Atieh Ranjbar Kermany, Afzaal Qamar, Jisheng Han, Takahiro Namazu, Ryutaro Maeda, Dzung Viet Dao, and Nam-Trung Nguyen

Citation: *Appl. Phys. Lett.* **110**, 141906 (2017); doi: 10.1063/1.4979834

View online: <http://dx.doi.org/10.1063/1.4979834>

View Table of Contents: <http://aip.scitation.org/toc/apl/110/14>

Published by the [American Institute of Physics](#)

---

### Articles you may be interested in

[Patterning the two dimensional electron gas at the LaAlO<sub>3</sub>/SrTiO<sub>3</sub> interface by structured Al capping](#)  
Applied Physics Letters **110**, 141603 (2017); 10.1063/1.4979784

[Quantum interference of two photons emitted from a luminescence center in GaAs:N](#)  
Applied Physics Letters **110**, 152102 (2017); 10.1063/1.4979520

[Oxidation induced stress in SiO<sub>2</sub>/SiC structures](#)  
Applied Physics Letters **110**, 141604 (2017); 10.1063/1.4979544

[Controlling phase of microwaves with active graphene surfaces](#)  
Applied Physics Letters **110**, 161102 (2017); 10.1063/1.4980087

[Optical probing of the Coulomb interactions of an electrically pumped polariton condensate](#)  
Applied Physics Letters **110**, 151103 (2017); 10.1063/1.4979836

[Experimental demonstration of fresh bunch self-seeding in an X-ray free electron laser](#)  
Applied Physics Letters **110**, 154101 (2017); 10.1063/1.4980092

---

**AIP** | Applied Physics  
Letters

Save your money for your research.  
It's now **FREE** to publish with us -  
no page, color or publication charges apply.

If your article has the  
potential to shape the future of  
applied physics, it BELONGS in  
*Applied Physics Letters*

## Ultra-high strain in epitaxial silicon carbide nanostructures utilizing residual stress amplification

Hoang-Phuong Phan,<sup>1,a)</sup> Tuan-Khoa Nguyen,<sup>1</sup> Toan Dinh,<sup>1</sup> Ginnosuke Ina,<sup>2</sup> Atieh Ranjbar Kermany,<sup>1</sup> Afzaal Qamar,<sup>1</sup> Jisheng Han,<sup>1</sup> Takahiro Namazu,<sup>3</sup> Ryutaro Maeda,<sup>4</sup> Dzung Viet Dao,<sup>1</sup> and Nam-Trung Nguyen<sup>1</sup>

<sup>1</sup>Queensland Micro and Nanotechnology Centre, Griffith University, Brisbane, QLD 4111, Australia

<sup>2</sup>Department of Mechanical Engineering, University of Hyogo, Hyogo 671-2280, Japan

<sup>3</sup>Department of Mechanical Engineering, Aichi Institute of Technology, Toyota 470-0392, Japan

<sup>4</sup>National Institute of Advanced Industrial Science and Technology (AIST), Tsukuba, Ibaraki 305-8560, Japan

(Received 22 February 2017; accepted 20 March 2017; published online 5 April 2017)

Strain engineering has attracted great attention, particularly for epitaxial films grown on a different substrate. Residual strains of SiC have been widely employed to form ultra-high frequency and high Q factor resonators. However, to date, the highest residual strain of SiC was reported to be limited to approximately 0.6%. Large strains induced into SiC could lead to several interesting physical phenomena, as well as significant improvement of resonant frequencies. We report an unprecedented nanostrain-amplifier structure with an ultra-high residual strain up to 8% utilizing the natural residual stress between epitaxial 3C-SiC and Si. In addition, the applied strain can be tuned by changing the dimensions of the amplifier structure. The possibility of introducing such a controllable and ultra-high strain will open the door to investigating the physics of SiC in large strain regimes and the development of ultra sensitive mechanical sensors. *Published by AIP Publishing.* [<http://dx.doi.org/10.1063/1.4979834>]

Strain engineering plays an important role in electronic devices.<sup>1,2</sup> For instance, in complementary metal oxide semiconductor (CMOS) technology, scaling down the device to the sub-100 nm regime encounters several challenges due to the degradation of carrier mobility.<sup>3,4</sup> To enhance the performance of silicon CMOSs with shrinking size, the introduction of strain into a Si channel has been a key concept to compensate the decrease in carrier mobility.<sup>5-7</sup> In addition, micro/nano-electromechanical systems (MEMSs/NEMSs) have also benefited from strain engineering where the residual strain was applied between epilayers to enhance the resonant frequency ( $f$ ) and the quality ( $Q$ ) factor following Euler-Bernoulli theory.<sup>8</sup>

Silicon carbide, a wide band gap material, has showed its high potential in MEMS/NEMS applications.<sup>9,10</sup> The large band gap makes SiC an excellent candidate for high temperature electronics applications where Si has limitation. The large Young's modulus of above 300 GPa offers SiC resonators higher resonant frequencies in comparison to their Si based counterparts.<sup>11,12</sup> Other physical properties such as the piezoresistive effect and the thermoresistive effect in SiC have also been employed to develop mechanical and thermal sensors for structural health monitoring (SHM).<sup>13-20</sup> Cubic SiC (3C-SiC) is the only polytype, among over 200 SiC polytypes, that can be grown (epitaxially) on the Si substrate and thus is the most suitable polytype for MEMS/NEMS applications.<sup>9,21</sup> This allows the reduction of the SiC/Si wafer cost as well as makes it compatible with the conventional micromachining process developed for Si. The epitaxial growth of SiC on Si further results in a large residual stress within the SiC film due to the lattice and thermal mismatches between the SiC film and the Si substrate.<sup>22</sup> This

residual stress can be potentially applied to enhance the  $f \times Q$  of the resonators. Resonators with high frequencies up to several GHz and  $f \times Q$  factors up to  $10^{11}$  have been developed through the application of residual stress.<sup>22-24</sup>

In most previous studies, the maximum strain induced into SiC ranged from 0.1% to 0.6%.<sup>27-30</sup> It should be noted that by inducing a larger strain, a higher resonant frequency can be achieved. In addition, large strains up to 10% could also lead to several significant changes in electrical/optical properties, which have been observed in several materials.<sup>31-33</sup> A large stress could also cause unintended properties such as wafer bow and cracks, making the realization of the ultra-high strain in SiC a challenging issue. Therefore, in order to make an extremely high strain in SiC possible, it is important to locally amplify strain in a specific area, while keeping the strain in the other parts of the film in a relatively small regime.

We here propose a method to induce an extremely high strain into SiC by using a nanostrain-amplifier. For the proof of concept, we demonstrate the feasibility of introducing a strain of approximately 8% into a SiC nano-spring structure, which is at least one order of magnitude larger than that reported in the literature. The possibility of inducing such a high strain will pave the way for experimental investigations of the physics of SiC in high strain regimes as well as for the development of highly sensitive SiC sensors. Our methodology should also be applicable for not only SiC but also other materials including graphene and transition metal dichalcogenides (TMDs), where high strain regimes are of significant interest.

Figure 1(a) illustrates the basic concept to induce a large strain into SiC devices. The nanostrain-amplifier consists of a SiC microbridge which is released from a Si substrate and a modified area which is located at the centre of the bridge.

<sup>a)</sup>Electronic mail: [hoangphuong.phan@griffithuni.edu.au](mailto:hoangphuong.phan@griffithuni.edu.au)

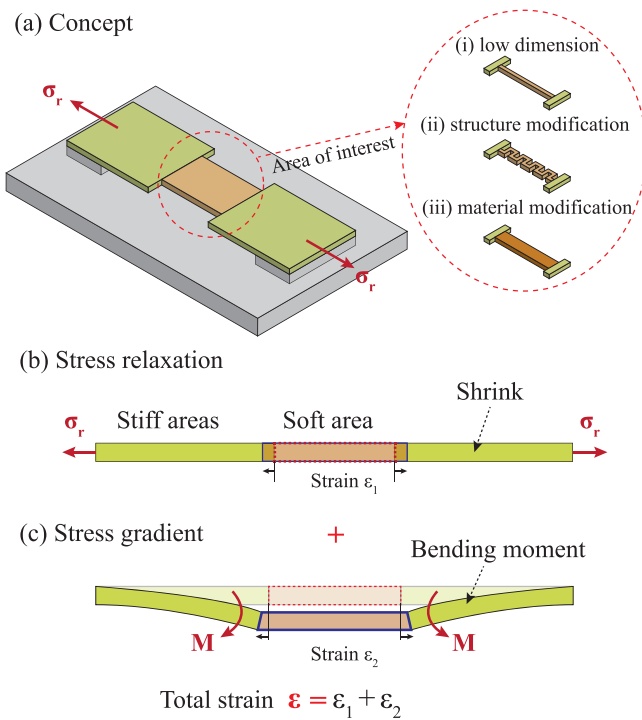


FIG. 1. (a) Concept of devices to induce a large strain into the interested area; (b), (c) Principle of the nanostrain-amplifier based on the planar residual stress and stress gradient (side-view sketch).

In addition, the modified area is designed to exhibit a smaller stiffness in comparison to the remaining areas of the SiC bridge. To soften this modified area, the following techniques can be utilized. First, the width of the middle area can be shrunk down to the nanometer scale so that the ratio of the stiffness between the nanowire and the micro-frame is significantly diminished. Second, the middle section can be softened by modifying its structure as such a nano-spring can offer much larger elongation than a nanorod with the same dimension. Furthermore, by changing the material from single-crystalline to amorphous, it is also possible to tune the stiffness of a specific region.<sup>25,26</sup> In the subsequent experiment, we selected the structure modification approach to form the soft area as it can provide large elongation which eases the strain observation using scanning electron microscopy (SEM).

The key finding of our structure is that the low stiffness of the modified nano-area allows it to follow the deformation of the serially connected microstructures. As 3C-SiC has a smaller lattice size than Si, the SiC film typically undergoes a considerable tensile stress when being epitaxially grown on the Si substrate. When a SiC bridge is released, its lattice constant tends to return to its original size, which subsequently shrinks the size of the bridge. Because this phenomenon is more dominant in the SiC micro-areas, the nano-areas will be stressed following the motion of these micro-areas, Fig. 1(b). Furthermore, in an epitaxial film, large stresses typically distribute near the interface between the top layer and the substrate. The residual stress gradually decreases with increasing film thickness or even relaxes for sufficiently thick films. This variation of the residual stress will cause a stress gradient along the thickness dimension, resulting in a bending moment once the film is suspended from the substrate. Therefore,

under the residual bending moment, the micro-frames will deflect vertically, leading to an elongation in the softened nano-area, Fig. 1(c). Combining the two phenomena of in-plane shrinking and out-of-plane deflection, an ultra-high strain is expected to be induced into the SiC nanostructures.

The SiC film was prepared on a Si (100) wafer using low pressure chemical vapor deposition (CVD) where silane ( $\text{SiH}_4$ ) and propylene ( $\text{C}_3\text{H}_6$ ) were employed as the precursors.<sup>35</sup> As aforementioned, SiC and Si have a significant lattice and a thermal expansion mismatch of  $\sim 20\%$  and  $\sim 8\%$ , respectively. The growth temperature was kept at  $1000^\circ\text{C}$  utilizing the alternating supply epitaxy (ASE) approach. The X-Ray Diffraction (XRD) method was utilized to investigate the crystallinity of the SiC film. Figure 2(a) shows diffraction peaks at  $35.6^\circ$  and  $90^\circ$ , corresponding to 3C-SiC(200) and 3C-SiC(400) orientations. In addition, besides these two peaks, only a peak at  $69.1^\circ$  was observed, corresponding to Si(400). This result indicated that single crystalline 3C-SiC (100) was grown on a Si substrate. The thickness of the films was found to be 294 nm using a NANOMETRICS Nanospec/AFT 210.

The Raman scattering measurement was performed using <sup>TM</sup>Renishaw inVia Raman microscope with a wavelength of 514 nm, Fig. 2(b). The peak observed at  $794\text{ cm}^{-1}$  corresponds to the transverse optical (TO) vibration of 3C-SiC. Our TO peak was relatively smaller than that of stress-free 3C-SiC which was reported to be  $795.9\text{ cm}^{-1}$ . Therefore, the left shift of the TO peak indicates the existence of a tensile stress in the epitaxial 3C-SiC film. The average tensile strain ( $\epsilon_r$ ) in the SiC film can be quantified using the coefficient reported by Rohmfeld *et al.*<sup>27</sup>

$$\frac{\omega_{TO}}{\text{cm}^{-1}} = (795.9 \pm 0.1) - (1125 \pm 20)\epsilon_r. \quad (1)$$

Consequently, the average strain induced into the as-deposited SiC film was approximately 0.16% to 0.2%, which

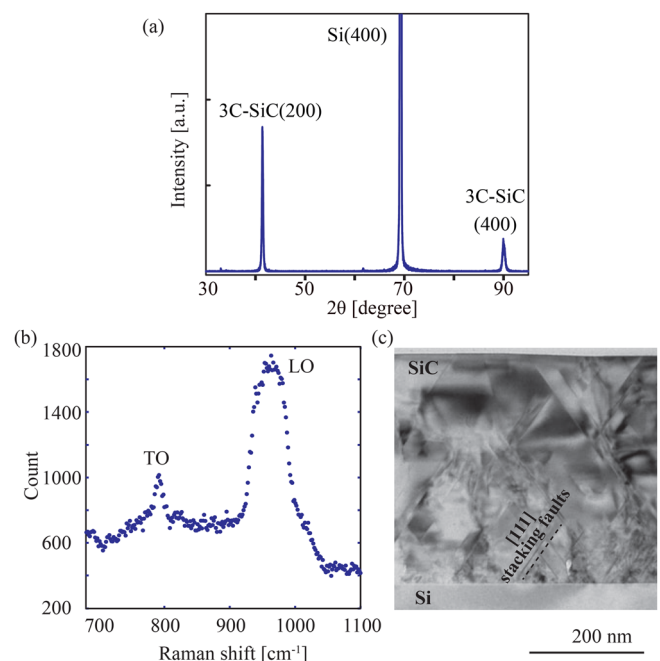


FIG. 2. Properties of the SiC films. (a) X-Ray Diffraction; (b) Raman spectroscopy; (c) Transmission electron microscopy.

was in the same range as that of the other epitaxial 3C-SiC films reported previously. Once the SiC bridge was suspended, the residual stress was released and SiC tended to return to its stress-free state. Furthermore, as the SiC microframes are much harder than the nano-spring (or other nanostructures) located at the centre, the shrink of these frames is much more dominant. Assuming that the microframes completely shrink down to their strain-free state, the strain induced into the nano-spring ( $\epsilon_{ns}$ ) can be approximated using the following equation:

$$\epsilon_{ns} = \frac{L_f}{L_{ns}} \epsilon_r, \quad (2)$$

where  $L_f$  and  $L_{ns}$  are the length of the frame and the nano-spring, respectively.

Additionally, the quality of the SiC film was characterized using transmission electron microscopy (TEM). The TEM image shown in Fig. 2(c) indicates the high density of defects near the SiC/Si interface. Most defects were found to be stacking faults in [111] crystallographic orientation due to the lattice mismatch between SiC and Si. The quality of the SiC film was evidently improved with the increasing film thickness, exhibiting less crystal defects on the top layers. This observation also indicates a stress gradient throughout the film. As such, in our previous report, a large stress was observed in the bottom layers of 3C-SiC (100) films, while the stress decreased or relaxed at layers near the top surface.<sup>34</sup> The bending moment exerted on SiC can be estimated from the Young's modulus of SiC and the deflection of free standing SiC cantilevers. Accordingly, the deflection ( $\delta$ ) of a suspended SiC cantilever is given by

$$\delta = \frac{Ml^2}{2EI}, \quad (3)$$

where  $M$  is the bending moment and  $l$ ,  $E$ , and  $I$  are the length, Young's modulus, and moment of inertia of the SiC cantilever. As a result, the bending moment caused by the stress gradient is given by:  $M = 2EI\delta/l^2$ . Figure 3 shows a large out-of-plane deflection of a SiC cantilever due to the residual stress gradient observed in Focused Ion Beam (FIB) equipment with a tilt

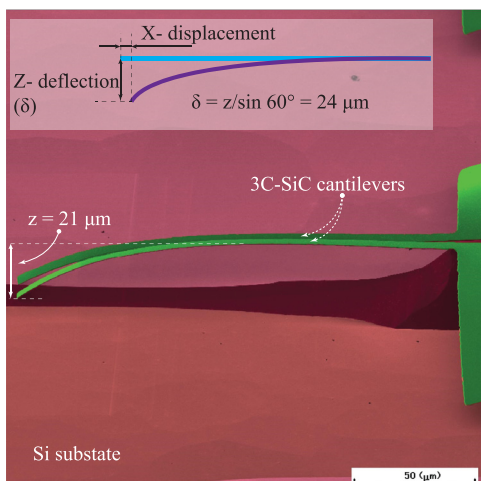


FIG. 3. Observation of the out-of-plane deflection in a released 3C-SiC cantilever due to the residual stress gradient (fall color).

angle of  $60^\circ$ . From the deflection of  $24 \mu\text{m}$ , the dimensions of the cantilever of  $200 \mu\text{m} \times 5 \mu\text{m} \times 0.3 \mu\text{m}$ , and the SiC Young's modulus of 350 GPa, the bending moment is estimated to be  $5 \mu\text{N} \mu\text{m}$ . Consequently, this relatively large bending moment exerted on the microframes in the nanostrain-amplifier would cause a large vertical displacement and thus results in a large tensile strain in the bridging nano-spring.

Figure 4(a) shows the fabrication process of the proposed devices. For the proof of concept, we used a spring structure since it offers a lower spring constant in comparison to nano-wires with the same width and thickness. The use of long SiC springs also allows a direct measurement of strains using a typical SEM. Initially, silicon carbide microstructures were patterned using inductive coupled plasma etching ( $\text{HCl} + \text{O}_2$ ) with an etching rate of approximately 100 nm/min.<sup>36</sup> The SiC bridges were then released from the substrate by under-etching Si using TMAH at  $90^\circ\text{C}$  for approximately 1 h (step 1). The width of the bridges was fixed at  $5 \mu\text{m}$ , while their length was varied from  $100 \mu\text{m}$  to  $500 \mu\text{m}$ . Consequently, SiC nano-springs and supporting wires were then formed at the middle of the bridge using a focused ion beam ( $\text{Ga}^+$ ) (step 2).<sup>37</sup> The length of the spring was  $27.71 \mu\text{m}$ , and the cross-sectional area was  $294 \text{ nm} \times 300 \text{ nm}$ . Finally, the supporting wires were removed by the FIB (step 3), releasing the nano-spring.

Figure 4(b) shows the SEM image of suspended SiC bridges prior to releasing the nano-spring. Evidently, the bridges were in an almost flat shape, indicating a uniform strain contributing along its longitudinal direction. Figure 4(c) presents the SEM image of the nano-spring after removing the supporting wires. The microcantilevers on each side of the bridge were deflected vertically, leading to a large displacement in the nano-spring. Furthermore, the cantilevers were bent downward, indicating that a large compressive stress is distributed at the bottom layer with respect to that of the top layers, Fig. 4(d). This result was in good agreement with the TEM observation mentioned above. Interestingly, because the two cantilevers were deflected at almost the same degree, the nano-spring remained in the lateral plane. Therefore, the length of the nano-spring can be accurately measured from the top view SEM image. In addition, as shown in Figure 4(e), to represent the visibility of large strains induced using the proposed structure, we fabricated a pair of nanosprings in which one was completely released (top), while the other one was supported on both the sides using two microwires (bottom). Accordingly, a significant increase in the length of the nanospring was observed after removing the supporting wires. Let  $L$  and  $\Delta L$  be the initial length and the elongation of the nanospring observed using SEM, respectively; the induced strain is estimated to be  $\epsilon = \Delta L/L$ .

Figure 5 plots the strain in SiC nano-springs against the ratio between the length of the nano-spring and that of the suspended bridge ( $L_{ns}/L_f$ ). A strain of 7.6% in the SiC nano-spring was observed when  $L_{ns}/L_f$  was 0.055, which is the largest strain reported in SiC so far. Additionally, increasing the  $L_{ns}/L_s$  results in a decrease in the applied strain, which is in solid agreement with Eqs. (2) and (3). More importantly, the dependence of the strain of the nano-spring on  $L_{ns}/L_f$  indicates that the ultra-high strain is controllable by changing

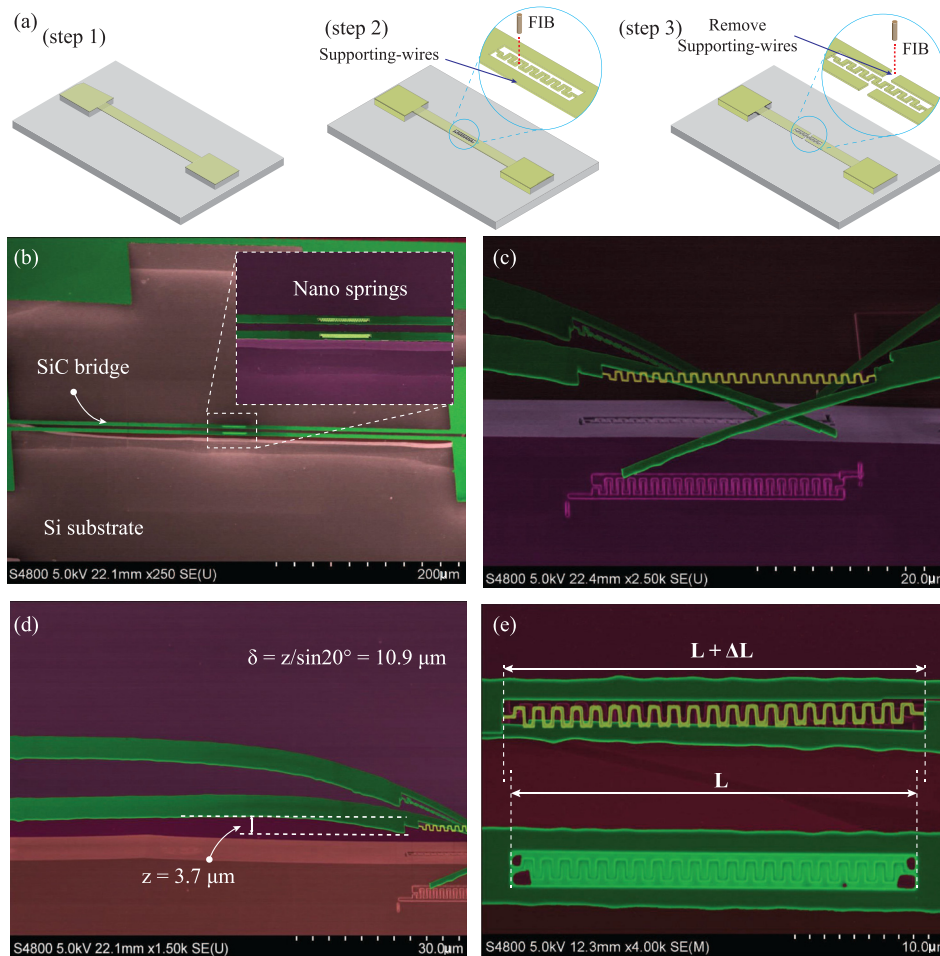


FIG. 4. Fabrication and SEM images of SiC nano-springs. (a) Fabrication process; (b) suspended SiC bridge with the nano-spring fabricated at the center (prior to removing the supporting wires); (c) SiC nano-springs after cutting the supporting wires; (d) deflection of the microframe (or cantilever) on each side; (e) the elongation of the nano-spring observed from the top view.

the device dimensions. This could be applied to tune the resonant frequency in SiC nanoresonators.

Another interesting property of our nano-strain amplifier is that the strain was only concentrated in the locally formed nano-spring, while the microframe (i.e., the SiC cantilever on each side of the bridge) can be almost freely deformed to release the residual stress. This means that the strain can be solely amplified at interested segments, retaining initially a small strain in others. Therefore, the proposed structure can be applied to locally induce an extremely high strain into 2D materials such as graphene or transition metal dichalcogenides,

where the van der Waals adhesion force between them and the substrate (e.g., Si, PDMS, and glass) typically cannot withstand 1% strain.<sup>38–41</sup> It should also be pointed out that as 2D materials typically have only a few atomic layers, the stress gradient is expected to be negligible. Therefore, the strain amplification in these materials is considered to be dominated by the in-plane compression of microframes with respect to the locally fabricated nanostructures, as described in Eq. (2). The capability of inducing ultra-high residual strains into 2D materials could open up promising possibilities for the development of high frequency and high Q factor nanoresonators.<sup>42–44</sup>

In conclusion, this work has presented a mechanical approach to apply an extremely large strain to SiC utilizing a nanostrain-amplifier and the residual stress. We demonstrated an extremely high strain up to nearly 8% in a SiC nano-spring structure. The proposed platform shows its potential for further investigations into the physics of SiC nanostructures in high strain regimes, as well as the development of high frequency, high Q factor, and ultra-sensitive SiC mechanical sensors.

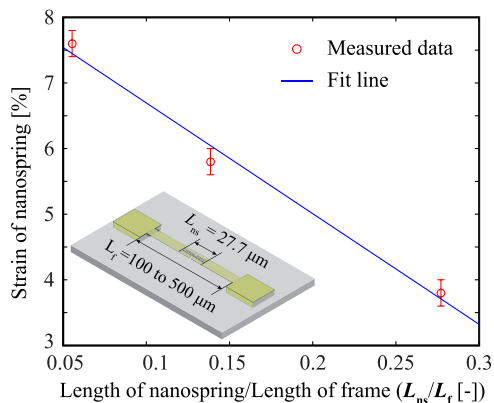


FIG. 5. Strain in SiC nano-springs with different  $L_{ns}/L_f$  ratios. For the same  $L_{ns}$ , increasing the length of the SiC bridge  $L_f$  leads to an increase in the strain of the nano-spring.

This work was partially funded by the linkage grant (LP150100153) from the Australian Research Council (ARC). This work was performed in part at the Queensland node of the Australian National Fabrication Facility, a company established under the National Collaborative Research Infrastructure Strategy to provide nano- and micro-fabrication facilities for Australia's researchers.

- <sup>1</sup>C. Si, Z. Sun, and F. Liu, *Nanoscale* **8**(6), 3207–3217 (2016).
- <sup>2</sup>Y. Zhang, C. Liu, J. Liu, J. Xiong, J. Liu, K. Zhang, Y. Liu, M. Peng, A. Yu, A. Zhang, Y. Zhang, Z. Wang, J. Zhai, and Z. L. Wang, *ACS Appl. Mater. Interfaces* **8**(2), 1381–1387 (2016).
- <sup>3</sup>Y. M. Niquet, C. Delerue, and C. Krzeminski, *Nano Lett.* **12**(7), 3545–3550 (2012).
- <sup>4</sup>S. W. Bedell, A. Khakifirooz, and D. K. Sadana, *MRS Bull.* **39**(02), 131–137 (2014).
- <sup>5</sup>X. L. Feng, R. He, P. Yang, and M. L. Roukes, *Nano Lett.* **7**(7), 1953–1959 (2007).
- <sup>6</sup>M. K. Zalalutdinov, J. T. Robinson, C. E. Junkermeier, J. C. Culbertson, T. L. Reinecke, R. Stine, and E. S. Snow, *Nano Lett.* **12**(8), 4212–4218 (2012).
- <sup>7</sup>B. Witkamp, M. Poot, and H. S. van der Zant, *Nano Lett.* **6**(12), 2904–2908 (2006).
- <sup>8</sup>R. B. Karabalin, L. G. Villanueva, M. H. Matheny, J. E. Sader, and M. L. Roukes, *Phys. Rev. Lett.* **108**(23), 236101 (2012).
- <sup>9</sup>H.-P. Phan, D. V. Dao, K. Nakamura, S. Dimitrijević, and N.-T. Nguyen, *J. Microelectromech. Syst.* **24**(6), 1663–1677 (2015).
- <sup>10</sup>D. G. Senesky, B. Jamshidi, K. B. Cheng, and A. P. Pisano, *IEEE Sens. J.* **9**(11), 1472–1478 (2009).
- <sup>11</sup>Y. Matsuda, N. Kim, S. W. King, J. Bielefeld, J. F. Stebbins, and R. H. Dauskardt, *ACS Appl. Mater. Interfaces* **5**(16), 7950–7955 (2013).
- <sup>12</sup>K. Brueckner, F. Niebelschuetz, K. Tonisch, Ch. Foerster, V. Cimalla, R. Stephan, J. Pezoldt, T. Stauden, O. Ambacher, and M. A. Hein, *Phys. Status Solidi A* **208**(2), 357–376 (2011).
- <sup>13</sup>A. Qamar, H.-P. Phan, D. V. Dao, P. Tanner, T. Dinh, L. Wang, and S. Dimitrijević, *IEEE Electron Device Lett.* **36**(7), 708–710 (2015).
- <sup>14</sup>F. Gao, J. Zheng, M. Wang, G. Wei, and W. Yang, *Chem. Commun.* **47**(43), 11993–11995 (2011).
- <sup>15</sup>D. V. Dao, H.-P. Phan, A. Qamar, and T. Dinh, *RSC Adv.* **6**(26), 21302–21307 (2016).
- <sup>16</sup>J. Bi, G. Wei, L. Wang, F. Gao, J. Zheng, B. Tang, and W. Yang, “Highly sensitive piezoresistance behaviors of n-type 3C-SiC nanowires,” *J. Mater. Chem. C* **1**(30), 4514–4517 (2013).
- <sup>17</sup>N. Zhang, C. M. Lin, D. G. Senesky, and A. P. Pisano, *Appl. Phys. Lett.* **104**(7), 073504 (2014).
- <sup>18</sup>T. Dinh, H.-P. Phan, T. Kozeki, A. Qamar, T. Namazu, N.-T. Nguyen, and D. V. Dao, *RSC Adv.* **5**, 106083–106086 (2015).
- <sup>19</sup>S. Rao, G. Pangallo, F. Pezzimenti, and F. G. Della Corte, *IEEE Electron Device Lett.* **36**(7), 720–722 (2015).
- <sup>20</sup>T. Dinh, D. V. Dao, H.-P. Phan, L. Wang, A. Qamar, N.-T. Nguyen, P. Tanner, and M. Rybachuk, *Appl. Phys. Express* **8**(6), 061303 (2015).
- <sup>21</sup>H. P. Phan, T. Dinh, T. Kozeki, T. K. Nguyen, A. Qamar, T. Namazu, N.-T. Nguyen, and D. V. Dao, *IEEE Electron Device Lett.* **37**(8), 1029–1032 (2016).
- <sup>22</sup>X. M. H. Huang, C. A. Zorman, M. Mehregany, and M. L. Roukes, *Nature* **421**(6922), 496–496 (2003).
- <sup>23</sup>A. R. Kermany, G. Brawley, N. Mishra, E. Sheridan, W. P. Bowen, and F. Iacopi, *Appl. Phys. Lett.* **104**(8), 081901 (2014).
- <sup>24</sup>Z. Wang, J. Lee, and P. X. L. Feng, *Nat. Commun.* **5**, 5158 (2014).
- <sup>25</sup>T. Kozeki, H. P. Phan, D. V. Dao, S. Inoue, and T. Namazu, *Jpn. J. Appl. Phys., Part 1* **55**(6S1), 06GL02 (2016).
- <sup>26</sup>L. L. Snead and J. C. Hay, *J. Nucl. Mater.* **273**(2), 213–220 (1999).
- <sup>27</sup>S. Rohmfeld, M. Hundhausen, L. Ley, C. A. Zorman, and M. Mehregany, *J. Appl. Phys.* **91**, 1113–1117 (2002).
- <sup>28</sup>M. A. Capano, B. C. Kim, A. R. Smith, E. P. Kvam, S. Tsoi, and A. K. R. Ramdas, *J. Appl. Phys.* **100**(8), 083514 (2006).
- <sup>29</sup>R. Anzalone, A. Alberti, and F. La Via, *Mater. Lett.* **118**, 130–133 (2014).
- <sup>30</sup>G. Colston, S. D. Rhead, V. A. Shah, O. J. Newell, I. P. Dolbnya, D. R. Leadley, and M. Myronov, *Mater. Des.* **103**, 244–248 (2016).
- <sup>31</sup>M. R. Falvo, G. J. Clary, R. M. Taylor, V. Chi, F. P. Brooks, S. Washburn, and R. Superfine, *Nature* **389**(6651), 582–584 (1997).
- <sup>32</sup>R. Fei and L. Yang, *Nano Lett.* **14**(5), 2884–2889 (2014).
- <sup>33</sup>L. Tong, M. Mehregany, and L. G. Matus, *Appl. Phys. Lett.* **60**(24), 2992–2994 (1992).
- <sup>34</sup>A. R. Kermany and F. Iacopi, *J. Appl. Phys.* **118**(15), 155304 (2015).
- <sup>35</sup>H.-P. Phan, A. Qamar, D. V. Dao, T. Dinh, L. Wang, J. Han, P. Tanner, S. Dimitrijević, and N.-T. Nguyen, *RSC Adv.* **5**, 56377–56381 (2015).
- <sup>36</sup>H. P. Phan, T. Dinh, T. Kozeki, A. Qamar, T. Namazu, S. Dimitrijević, N.-T. Nguyen, and D. V. Dao, *Sci. Rep.* **6**, 28499 (2016).
- <sup>37</sup>H. P. Phan, T. Dinh, T. Kozeki, T. K. Nguyen, A. Qamar, T. Namazu, N.-T. Nguyen, and D. V. Dao, *Appl. Phys. Lett.* **109**(12), 123502 (2016).
- <sup>38</sup>H. H. Perez-Garza, E. W. Kievit, G. F. Schneider, and U. H. Staufer, *Nanotechnology* **25**(46), 465708 (2014).
- <sup>39</sup>H. Rostami, R. Roldan, E. Cappelluti, R. Asgari, and F. Guinea, *Phys. Rev. B* **92**(19), 195402 (2015).
- <sup>40</sup>J. Tao, W. Shen, S. Wu, L. Liu, Z. Feng, C. Wang, C. Hu, P. Yao, H. Zhang, W. Pang, X. Duan, J. Liu, C. Zhou, and D. Zhang, *ACS Nano* **9**(11), 11362–11370 (2015).
- <sup>41</sup>G. Plechinger, A. Castellanos-Gomez, M. Buscema, H. S. van der Zant, G. A. Steele, A. Kuc, T. Heine, C. Schuller, and T. Korn, *2D Mater.* **2**(1), 015006 (2015).
- <sup>42</sup>S. Shivaraman, R. A. Barton, X. Yu, J. Alden, L. Herman, M. V. S. Chandrashekar, J. Park, P. L. McEuen, J. M. Parpia, H. G. Craighead, and M. G. Spencer, *Nano Lett.* **9**(9), 3100–3105 (2009).
- <sup>43</sup>M. Takamura, K. Furukawa, H. Okamoto, S. Tanabe, H. Yamaguchi, and H. Hibino, *Jpn. J. Appl. Phys., Part 1* **52**(4S), 04CH01 (2013).
- <sup>44</sup>Y. Oshidari, T. Hatakeyama, R. Kometani, S. I. Warisawa, and S. Ishihara, *Appl. Phys. Express* **5**(11), 117201 (2012).